A new look at sulphur chemistry in hot cores and corinos

Thomas Vidal, Valentine Wakelam

Monthly Notices
of the
ROYAL ASTRONOMICAL SOCIETY

MNRAS **474,** 5575–5587 (2018) doi:10.1093/mnras/stx3113

A new look at sulphur chemistry in hot cores and corinos

Thomas H. G. Vidal★ and Valentine Wakelam

Laboratoire d'astrophysique de Bordeaux, Univ. Bordeaux, CNRS, B18N, allée Geoffroy Saint-Hilaire, F-33615 Pessac, France

Accepted 2017 November 28. Received 2017 November 28; in original form 2017 September 8

ABSTRACT

Sulphur-bearing species are often used to probe the evolution of hot cores because their abundances are particularly sensitive to physical and chemical variations. However, the chemistry of sulphur is not well understood in these regions, notably because observations of several hot cores have displayed a large variety of sulphur compositions, and because the reservoir of sulphur in dense clouds, in which hot cores form, is still poorly constrained. In order to help disentangle its complexity, we present a fresh comprehensive review of sulphur chemistry in hot cores along with a study of sulphur's sensibility to temperature and pre-collapse chemical composition. In parallel, we analyse the discrepencies that result from the use of two different types of models (static and dynamic) in order to highlight the sensitivity to the choice of model to be used in astrochemical studies. Our results show that the pre-collapse chemical composition is a critical parameter for sulphur chemistry in hot cores and that it could explain the different sulphur compositions observed. We also report that differences in abundances for a given species between the static and dynamic models can reach six orders of magnitude in the hot core, which reveals the key role of the choice of model in astrochemical studies.

Key words: astrochemistry – methods: numerical – stars: abundances – stars: formation – stars: protostars – ISM: molecules.

1 INTRODUCTION

Hot cores have been defined as small (<0.1 pc), dense ($n_H > 2 \times 10^7$ cm^{-3}) and warm ($T > 100$ K) regions surrounding high-mass protostars in their early phase of formation (see for example, Kurtz et al. 2000; van der Tak 2004). Because of their high temperatures, these regions are characterized by the sublimation of icy mantles of dust grain. Therefore, they present high abundances of hydrogenated molecules, such as water (H_2O), hydrogen sulfide (H_2S) or complex organic molecules such as methanol (CH_3OH; see Schöier et al. 2002, and references therein). These molecules are originally synthesized on dust grains in the cold dense cloud from which the protostar has formed. Once evaporated in the hot core, they undergo further gas-phase chemical reactions (Wakelam et al. 2004b; Garrod & Herbst 2006; Herbst & van Dishoeck 2009). It is now generally admitted that low-mass protostars present the same kind of physico-chemical structure called 'hot corinos' (Ceccarelli, Hollenbach & Tielens 1996; Ivezic & Elitzur 1997). They differ from their high-mass counterparts mainly in size and, consequently, in infall time-scale, which could perhaps affect the chemical composition. Because our Sun is a low-mass star, the chemistry that takes place in these 'small' hot cores is important for understanding the history of the material from which planetary systems such as ours are formed. In this paper, we use the expression 'hot core' as a generic term to designate the hot and dense regions surrounding both high-mass and low-mass protostars.

To model the chemistry of hot cores, several types of simulations exist in the literature (see for instance, Charnley 1997; Hatchell et al. 1998; Garrod & Herbst 2006; Wakelam, Hersant & Herpin 2011; Hincelin et al. 2016). Ranging from simple zero-dimensional static gas-phase models to complex three-dimensional gas-grain models, different assumptions are made for each type of model, regarding for instance the age of the parent cloud or its free-fall time. These numerous approaches to hot core chemistry and the different hypotheses they imply raise the question of the uniformity of the results obtained by these models.

Sulphur-bearing species are often used to probe the evolution of hot cores because their abundance is particularly sensitive to physical and chemical variations. For example, the ratios SO_2/SO, SO_2/H_2S and OCS/H_2S have been proposed as chemical clocks in these regions (Charnley 1997; Hatchell et al. 1998; Wakelam et al. 2011), SO is often used to trace small-scale heating process, such as shocked regions (Viti et al. 2001; Podio et al. 2015) or the centrifugal barrier (Sakai et al. 2014), and OCS can efficiently trace the infalling-rotating envelope (Oya et al. 2016).

Hence, the modelling of sulphur chemistry in such hot and dense regions is crucial for a better understanding of the star formation process. Moreover, such models can uncover new information on the main form of sulphur in dense clouds. Indeed, the gas-phase abundance of atomic sulphur in the diffuse medium is observed to be constant with cloud density, around its cosmic value of 10^{-5}

★ E-mail: thomas.vidal@u-bordeaux.fr

(see for instance, Jenkins 2009). However, in dense clouds, the total abundance of detected S-bearing molecules only accounts for 0.1 per cent of the cosmic abundance of atomic sulphur (Tieftrunk et al. 1994; Charnley 1997). Furthermore, for most chemical models, assuming an initial abundance of sulphur as high as its cosmic value results in predicted abundances of observable S-bearing species much higher than the observed abundances. Consequently, modellers usually assume a depleted abundance of sulphur compared to its cosmic value. Therefore, the main reservoirs of sulphur in dense clouds, and consequently in hot cores, are still uncertain.

Let us add to these uncertainties the fact that the observation of S-bearing species in hot cores is also a puzzling issue, as a large variety of sulphur compositions have been observed towards different hot cores and therefore no global trend has yet been found (see fig. 5 of Woods et al. 2015, and references therein). However, a given set of hot cores can present similar sulphur composition (see for example, Minh 2016), which would suggest similar evolutionary stages.

Recent studies have put forward evidence in favour of the long-lasting idea that because hydrogenation is the most effective chemical process in icy grain mantles, H_2S could be the sought-for main reservoir of sulphur in dense clouds (see Minh et al. 1990; Charnley 1997). Holdship et al. (2016) studied the properties of H_2S in the low-mass protostar L1157-B1 and showed that a significant fraction of the sulphur is likely to be locked into the form of H_2S prior to evaporation of the grain mantles in the hot corino. Moreover, we reported the first chemical model able to reproduce observed abundances of S-bearing species in dense clouds, using as an initial abundance of sulphur its cosmic abundance (or three times depleted; see Vidal et al. 2017). In this previous paper, we showed that the main form of sulphur in dense clouds critically depends on the age of the cloud. We proposed that this reservoir could be atomic sulphur for clouds of ages $<5 \times 10^5$ yr, or a shared reservoir between HS and H_2S in the grain mantles for older clouds.

In this current paper, we aim to present a comprehensive study of the modelling of S-bearing species in hot cores. In particular, we try to determine how the history (i.e. the pre-collapsing chemical composition) of a hot core affects sulphur chemistry, and how important is the choice of the type of model used for hot cores studies. Hence, we study the evolution of the abundances of the main S-bearing species observed in a hot core, as given by different types of simulations using several physico-chemical parameters. In Section 2, we present the gas grain model as well as the different types of simulations we run. In Section 3, we present the results of our hot core simulations for sulphur chemistry. We discuss these results regarding the issues we want to address in the final section.

2 MODEL DESCRIPTION

In order to conduct a comprehensive study of the sulphur chemistry in hot cores, as well as highlighting the discrepancies between the different models commonly used in the literature, we use three types of simulations:

(i) zero-dimensional simulations for which we consider constant physical parameters throughout the simulation time;
(ii) one-dimensional static simulations for which each cell of the spatial grid evolves with constant physical parameter as a zero-dimensional model;
(iii) zero-dimensional dynamic simulations for which each cell of the spatial grid evolves with time-dependant physical parameters.

For all the simulations, we use the latest version of the time-dependent gas-grain NAUTILUS V-1.1 chemical model (Ruaud, Wakelam & Hersant 2016). In the following, we describe the chemical model, and then we give the parameters of the parent cloud model we use to obtain the same pre-collapsing chemical composition for all hot cores models. Afterwards, we describe the different parameters we use for each simulation.

2.1 Chemical model

The NAUTILUS chemical model computes the evolution of chemical abundances for a given set of physical and chemical parameters. It can simulate a three-phase chemistry including gas-phase, grain-surface and grain-bulk chemistry, along with the possible exchanges between the different phases (Ruaud et al. 2016). These exchanges are: the adsorption of gas-phase species on to grain surfaces, the thermal and non-thermal desorption of species from the grain surface into the gas phase, and the surface–bulk and bulk–surface exchange of species. The chemical desorption process used in the model is the one depicted in Garrod, Wakelam & Herbst (2007). They considered that for each surface reaction leading to a single product, a part of the energy released by the reaction can contribute to the desorption of the product in the gas phase using the Rice–Ramsperger–Kessel theory. The fraction of the product desorbed in the gas phase depends on the binding energy of the product to the surface, the enthalpy of the reaction, and the fraction of the released energy that is lost to the surface. In our case, we use an a parameter of 0.001, which produces approximately a 1 per cent efficiency evaporation for all species. Moreover, the grain chemistry takes into account the standard direct photodissociation by photons along with the photodissociation induced by secondary UV photons introduced by Prasad & Tarafdar (1983). These processes are effective on the surface as well as in the bulk of the grains. The model also takes into account the newly implemented competition between reaction, diffusion and evaporation, as suggested by Chang, Cuppen & Herbst (2007) and Garrod & Pauly (2011). The diffusion energies of each species are computed as a fraction of their binding energies. We take for the surface a value of this ratio of 0.4 as suggested by experiments and theoretical work made on H (see Ruaud et al. 2016, and reference therein), CO and CO_2 (see Karssemeijer & Cuppen 2014). This value is then extrapolated to every species on the surface. For the bulk, we take a value of 0.8 (see also Ruaud et al. 2016).

Given the high-temperature regimes encountered in this study, we use the ad hoc formation mechanism for H_2 described in Harada, Herbst & Wakelam (2010). They consider that the formation rate of H_2 can be written as

$$\frac{\mathrm{d}n(\mathrm{H_2})}{\mathrm{d}t} = \frac{1}{2} n_{\mathrm{H}} v_{\mathrm{H}} n_{\mathrm{g}} \sigma_{\mathrm{g}} S(T) \epsilon, \quad (1)$$

where n_{H} and v_{H} are the number density and thermal velocity of hydrogen atoms, respectively, in part cm^{-3} and cm s^{-1}, n_{g} is the number density of grains in part cm^{-3}, σ_{g} is the cross-section of a grain in cm^2, S is the sticking coefficient for a hydrogen atom as a function of temperature and ϵ is the recombination efficiency. For our study, we use for the recombination efficiency the results from Cazaux et al. (2005), and for the sticking coefficient the expression derived by Chaabouni et al. (2012).

The reference chemical networks are *kida.uva.2014* (see Wakelam et al. 2015a) for the gas phase and that described in Ruaud et al. (2016) for the grains. To this we added the sulphur network detailed in Vidal et al. (2017) (including the reactions given in Druard & Wakelam 2012), as well as the chemical schemes for carbon chains proposed in Wakelam et al. (2015b), Loison et al. (2016, 2017) and

Table 1. Initial abundances. In the n_i/n_H column, $a(b)$ stands for $a \times 10^b$. References are: 1, Wakelam & Herbst (2008); 2, Jenkins (2009); 3, Hincelin et al. (2011); 4, low-metal abundances from Graedel, Langer & Frerking (1982); 5, depleted value from Neufeld, Wolfire & Schilke (2005).

Element	n_i/n_H	References
H_2	0.5	
He	0.09	1
N	6.2(−5)	2
O	2.4(−4)	3
C^+	1.7(−4)	2
S^+	1.5(−5)	2
Si^+	8.0(−9)	4
Fe^+	3.0(−9)	4
Na^+	2.0(−9)	4
Mg^+	7.0(−9)	4
P^+	2.0(−10)	4
Cl^+	1.0(−9)	4
F	6.7(−9)	5

Hickson, Wakelam & Loison (2016). Note that all abundances in this paper are expressed with respect to the total H density.

2.2 Parent cloud parameters

In order to model the chemistry of a given hot core, one must consider as an initial condition the chemical composition of its parent cloud before it collapses. Moreover, if we want to be able to compare the outputs of our different types of simulations, it makes sense to use the same initial chemical composition. Hence, we begin to run a simulation with the commonly used dark cloud physical parameters: a gas and dust temperature of 10 K, an atomic hydrogen total density of 2×10^4 cm^{-3}, a cosmic ionization rate of 1.3×10^{-17} s^{-1} and a visual extinction of 15 mag. Our set of initial abundances is summarized in Table 1. We start with all species in their atomic (or ionized) form, except for hydrogen, which is assumed to be entirely in its molecular form. As our model does not require additional depletion of sulphur from its cosmic value to reproduce dark cloud observations (Vidal et al. 2017), we choose to use it as an initial abundance of sulphur.

We show that the evolution time of the parent cloud is critical for the sulphur reservoirs (Vidal et al. 2017) and the same kind of results is observed for oxygen in our simulations. Hence, in order to study the importance of the chemical history of the parent cloud on the hot core composition, we use the outputs of the parent cloud simulation at two different final times for all our simulations: 10^5 and 10^6 yr. Both these ages are acceptable for dark clouds and allow us to obtain two very different chemical compositions of the cloud before it collapses. On the one hand, in the case of the less evolved dark cloud (hereafter LEDC), most of the oxygen and sulphur are still in the gas phase in atomic form (42 and 61 per cent of their total amount, respectively), or in the form of CO (26 per cent) and CS (15 per cent), respectively. The remainder is, for both species, locked in icy grain bulks, mainly in the form of H_2O, HS and H_2S. On the other hand, in the case of the evolved dark cloud (hereafter EDC), more than 95 per cent of the oxygen is locked in the ices mainly in the form of H_2O (53 per cent) and H_2CO (9 per cent). As for sulphur, more than 90 per cent is locked in the ices, including its main reservoirs HS (35 per cent) and H_2S (26 per cent). The two pre-collapse cloud compositions are summarized in Table 2. For more details on the time evolution of the abundances of the main S-bearing species in the parent cloud, see fig. 1 of Vidal et al. (2017).

Table 2. Description of the pre-collapse dark cloud oxygen and sulphur composition. The prefix 'b-' denotes the bulk species.

LEDC	
Oxygen	Sulphur
O (42 per cent)	S (61 per cent)
CO (26 per cent)	CS (15 per cent)
b-H_2O (22 per cent)	b-HS (6 per cent)
b-O (1 per cent)	b-H_2S (5 per cent)
EDC	
Oxygen	Sulphur
b-H_2O (53 per cent)	b-HS (35 per cent)
b-H_2CO (9 per cent)	b-H_2S (26 per cent)
b-CO (8 per cent)	b-NS (17 per cent)
b-CH_3OH (7 per cent)	b-S (8 per cent)

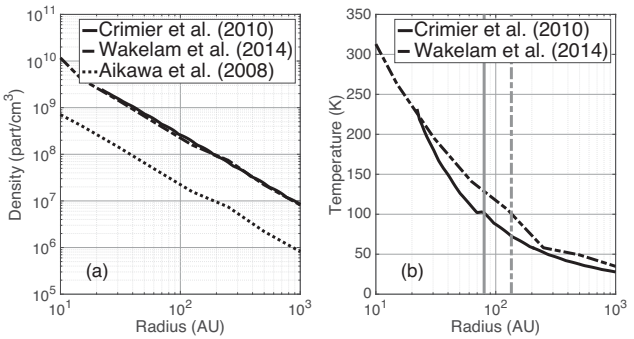

Figure 1. Radial structure of the one-dimensional static and zero-dimensional dynamic models at the final time for (a) density, for which we plot the initial structure from Aikawa et al. (2008) as reference, and (b) temperature, for which we plot the limit of the hot core ($T > 100$ K) for the one-dimensional static ($R_{HC} = 80$ au, solid grey vertical line) and zero-dimensional dynamic ($R_{HC} = 135$ au, dashed grey vertical line) models.

2.3 Zero-dimensional simulation parameters

For this study, we begin to run zero-dimensional simulations with the main purpose of obtaining a comprehensive look at sulphur chemistry in hot cores. As Charnley (1997) showed the important role of temperature on sulphur chemistry in such environments, we present calculations for a typical hot core density of 2×10^7 cm^{-3}, and two temperature regimes of 100 and 300 K. Hence, we obtain four zero-dimensional simulations with different pre-evaporative compositions (EDC and LEDC) and temperatures (100 and 300 K).

2.4 One-dimensional static simulation parameters

The one-dimensional model used in this paper follows the physical structure for the envelope of the low-mass protostar IRAS 16293–2422 from Crimier et al. (2010), which was constrained through multiwavelength dust and molecular observations. Indeed, this protostar is believed to have a hot core within ∼150 au around its centre (see Schöier et al. 2002). The density and temperature radial evolutions are shown in Figs 1(a) and (b), respectively (solid lines). For this model, the spatial limit of the hot core ($T > 100$ K) is located at $R_{HC} = 80$ au (solid grey line in Fig. 1b).

Table 3. Summary of the simulations designations and physical parameters.

Simulation	Physical parameter	Pre-collapse evolution time
	Zero-dimensional static models	
0DS100LEDC	$T = 100$ K, $n_H = 2 \times 10^7$ cm^{-3}	10^5 yr
0DS300LEDC	$T = 300$ K, $n_H = 2 \times 10^7$ cm^{-3}	10^5 yr
0DS100EDC	$T = 100$ K, $n_H = 2 \times 10^7$ cm^{-3}	10^6 yr
0DS300EDC	$T = 300$ K, $n_H = 2 \times 10^7$ cm^{-3}	10^6 yr
	One-dimensional static models	
1DSLEDC	Structure from Crimier et al. (2010)	10^5 yr
1DSEDC	Structure from Crimier et al. (2010)	10^6 yr
	Zero-dimensional dynamic models	
0DDLEDC	Modified structure from Aikawa et al. (2008)	10^5 yr
0DDEDC	Modified structure from Aikawa et al. (2008)	10^6 yr

2.5 Zero-dimensional dynamic simulation parameters

The structure we use for our dynamic simulation is the same as in Aikawa et al. (2008), Wakelam et al. (2014) and Majumdar et al. (2016), and it was computed from the radiation hydrodynamic (RHD) model of Masunaga & Inutsuka (2000). It initially starts from a parent cloud with a central density of $\sim 6 \times 10^4$ cm^{-3}, a radius of 4×10^4 au and a total mass of 3.852 $M_\odot$. Then the model follows the collapse of the pre-stellar core, which eventually forms a protostellar core after 2.5×10^5 yr. Finally, the protostar grows by mass accretion from the envelope for 9.3×10^4 yr. As in Wakelam et al. (2014), we have multiplied by 10 all the densities of the simulations in order for the final physical structure of the dynamic model to be similar to the one-dimensional structure of Crimier et al. (2010). The consequence of this modification is discussed in Section 4.1 (see also section 4.5 of Wakelam et al. 2014). Fig. 1(a) shows the resulting final density radial evolution (dashed line) as well as the previous one (dotted line), and Fig. 1(b) shows the final temperature radial evolution (dashed line). For this model, the spatial limit of the hot core ($T > 100$ K) is located at $R_{HC} = 135$ au (dashed grey line in Fig. 1b).

The designations and physical parameters of all the simulations presented in this paper are summarized in Table 3.

3 RESULTS

3.1 Zero-dimensional models

In this section, we aim to perform a comprehensive study of sulphur chemistry in environments such as hot cores. In particular, we want to address the importance of the temperature as well as the pre-collapse chemical composition using the four zero-dimensional simulations defined in Section 2.3. Sulphur chemistry in the hot gas phase is known to be intertwined with the distribution of reactive oxygen: O, O_2 and OH (Charnley 1997; Esplugues et al. 2014; Wakelam et al. 2004b). Hence, we begin with a description of the chemistry of these species, and then we study the chemistry of the main S-bearing species observed towards hot and dense objects: SO, SO_2, H_2S, OCS, CS and H_2CS.

3.1.1 Oxygen chemistry

The left, middle and right panels of Fig. 2 show the abundances of O, O_2 and OH, respectively, for the LEDC (top) and EDC (bottom) pre-collapse compositions. For atomic oxygen in the 0DS100LEDC case (see Fig. 2a), the temperature is not high enough for all the mantle of grain to evaporate and O reacts mainly with the S-bearing species available in the gas phase. It initially reacts with CS, which is the second most abundant S-bearing species in the gas phase, to form S and CO. As the abundance of CS consequently decreases, O is then mainly destroyed through formation of SO and SO_2:

$$O + S_2 \rightarrow S + SO \quad (2)$$

$$O + SO \rightarrow SO_2. \quad (3)$$

In the 0D300LEDC case (see Fig. 2a), the temperature of the core is high enough for mantle hydrocarbons (H_xC_n) to evaporate. They participate in the consumption of O by forming mainly CO, causing the O abundance to decrease much faster than in the 0D100LEDC case. However, the most efficient reaction at this temperature is

$$O + H_2 \rightarrow H + OH. \quad (4)$$

Towards the end ($t > 10^6$ yr), the abundance of atomic oxygen increases again from the reaction

$$CO + He^+ \rightarrow He + O + C^+, \quad (5)$$

as well as photodissociation by secondary UV photons of SO and SO_2.

With the pre-collapse composition of the EDC, contrary to the LEDC, most of the oxygen is trapped in grain mantle, mainly under the form of H_2O, H_2CO and CO (see Table 2). Hence, little atomic oxygen is available in the gas phase even after sublimation of the grain mantle, which explains the fact that its initial abundance in both EDC cases is lower by two orders of magnitude compared to LEDC cases. In the 0DS100EDC case (see Fig. 2d), the temperature of the corino is hot enough to sublimate light species, especially HS and NS, which are two of the sulphur reservoirs in the pre-collapse composition. These species react rapidly with O to form SO and NO for 10^4 yr. After this time, it is HCNS that reacts mainly with atomic oxygen through the following reactions:

$$O + HCNS \rightarrow HCN + SO \quad (6)$$

$$\rightarrow HCO + NS. \quad (7)$$

The global increase of abundance of O at the end of the simulation is due to reaction (5).

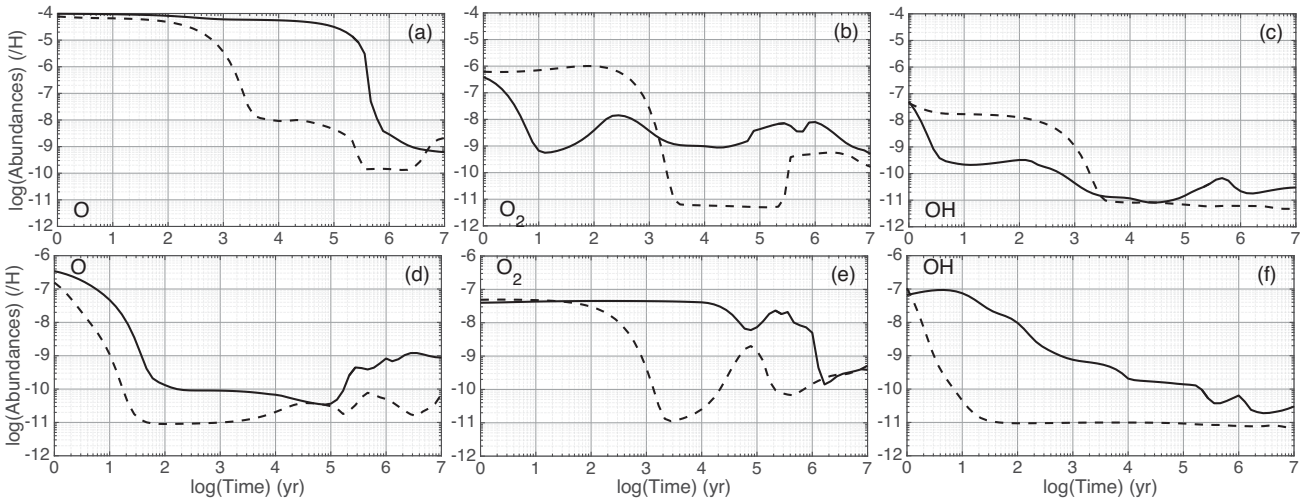

Figure 2. Abundances of O, O_2 and OH relative to H as a function of time for hot core conditions: $n_H = 2 \times 10^7$ cm^{-3} and $T = 100$ K (solid line) or 300 K (dashed line), and for LEDC (top panel) and EDC (bottom panel) pre-collapse compositions.

In the 0D300EDC case (see Fig. 2d), most of the sublimated hydrocarbons efficiently form CH_3, which consumes O in the first 100 yr following

$$O + CH_3 \rightarrow H + CO + H_2 \quad (8)$$

$$\rightarrow H + H_2CO. \quad (9)$$

Afterwards, O abundance increases slowly, mainly from the reaction

$$NH + NO \rightarrow H + O + N_2. \quad (10)$$

In both 0DS100LEDC and 0DS300LEDC models, dioxygen chemistry is strongly linked with S and OH chemistry via

$$S + O_2 \rightarrow O + SO \quad (11)$$

$$O + OH \rightarrow H + O_2. \quad (12)$$

At 100 K (see Fig. 2b), atomic carbon initially destroys O_2 faster than it is created by reaction (12) through

$$C + O_2 \rightarrow O + CO. \quad (13)$$

Then, atomic sulphur consumes both O_2 and OH (see Fig. 2c) within a time-scale of 1000 yr, respectively via reaction (11) and

$$S + OH \rightarrow H + SO. \quad (14)$$

Afterwards, the chemistries of both species are linked by reaction (12). The short increase of both abundances near 10^6 yr is mainly due to the formation of OH via electronic recombination of $HOCS^+$ and HSO_2^+.

At 300 K however (see Fig. 2b), atomic carbon is initially rapidly consumed by the two evaporated hydrocarbons C_4H_2 and C_2H_2, and does not destroy O_2 as efficiently as at 100 K. Instead, OH is formed rapidly via reaction (4) (see Fig. 2c), which causes the O_2 abundance to increase through reaction (12) in the first 100 yr. Then, O_2 and OH are consumed in a few 1000 yr, respectively, by reaction (11) and

$$H_2 + OH \rightarrow H + H_2O. \quad (15)$$

It should be noted that the increase in O_2 abundance near 10^5 yr is due to the following ion-neutral reactions:

$$S + O_2^+ \rightarrow O_2 + S^+ \quad (16)$$

$$SO_2 + He^+ \rightarrow He + O_2 + S^+. \quad (17)$$

In the EDC cases, atomic oxygen is not abundant enough in the gas phase for reaction (12) to be efficient. Hence, there is no evident link between O_2 and OH chemistries as in the LEDC cases. For the 0D100EDC model (see Fig. 2e), the abundance of dioxygen first slowly grows for a few 100 yr from the reaction:

$$HCO + O_2H \rightarrow O_2 + H_2CO. \quad (18)$$

O_2H is also destroyed by H to form OH, and when there is not enough left in the gas phase, HCO then reacts with O_2 causing its abundance to decrease after a few 1000 yr. Moreover, reaction (11) also becomes efficient after 10^4 yr and O_2 abundance starts to drop at this time. The increase near 10^5 yr is manly due to reaction (17).

In the 0D300EDC case (see Fig. 2e), the CH_3 formed from the evaporated hydrocarbon destroys efficiently O_2 for a few 1000 yr via

$$O_2 + CH_3 \rightarrow H_2O + HCO. \quad (19)$$

Afterwards, the abundance of O_2 globally increases from the following reactions:

$$O_3 + S \rightarrow SO + O_2 \quad (20)$$

$$O_2H + CH_3 \rightarrow CH_4 + O_2. \quad (21)$$

OH abundance generally decreases in both EDC models. For the 0D100EDC case (see Fig. 2f), this decrease is mainly due to

$$CS + OH \rightarrow H + OCS \quad (22)$$

$$H_2CO + OH \rightarrow H_2O + HCO. \quad (23)$$

As for the 0D300EDC case (see Fig. 2f), it is mainly due to reactions (15) and (23).

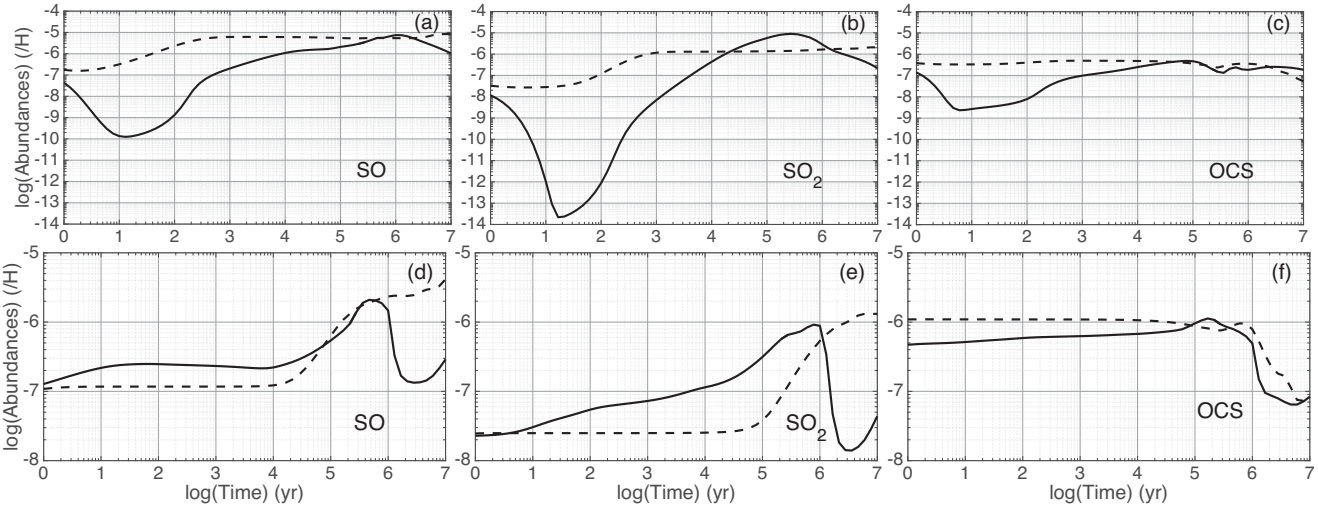

Figure 3. Abundances of SO, SO_2 and OCS relative to H as a function of time for hot core conditions: $n_H = 2 \times 10^7\,cm^{-3}$ and $T = 100\,K$ (solid line) and 300 K (dashed line), and for LEDC (top panel) and EDC (bottom panel) pre-collapse compositions.

3.1.2 Sulphur chemistry

In the following, we take a comprehensive look at the chemistry of the main neutral S-bearing species detected in hot cores, namely SO, SO_2, OCS, H_2S, H_2CS and CS.

SO, SO_2 and OCS in the LEDC cases

Fig. 3 displays the abundances of SO, SO_2 and OCS in both the LEDC (top panels) and EDC (bottom panels) cases. In the 0DS100LEDC case, these three species are initially destroyed by atomic carbon, which explains their respective drops in the first 10 yr of the simulation:

$$SO + C \rightarrow S + CO \quad (24)$$

$$\rightarrow O + CS \quad (25)$$

$$SO_2 + C \rightarrow SO + CO \quad (26)$$

$$OCS + C \rightarrow CS + CO. \quad (27)$$

SO abundance then grows, first mainly from reaction (14), then reactions (2) and (11) (see Fig. 3a). After 10^6 yr, as only a small mount of reactive oxygen remains in the gas phase, SO is no longer efficiently produced. It is instead mainly destroyed by CH through

$$SO + CH \rightarrow H + OCS \quad (28)$$

$$\rightarrow CO + HS. \quad (29)$$

SO_2 is linked with SO mainly by reaction (3), as well as

$$SO + OH \rightarrow H + SO_2, \quad (30)$$

which is only efficient when OH is abundant enough in the gas phase (i.e. at the very beginning of the simulation; see Fig. 2c). Hence, SO_2 abundance grows from 10 yr to a few 10^5 yr from these reactions (see Fig. 3b). Afterwards, SO_2 is destroyed by H_3^+ and C^+ following

$$SO_2 + H_3^+ \rightarrow H_2 + HSO_2^+ \quad (31)$$

$$SO_2 + C^+ \rightarrow CO + SO^+. \quad (32)$$

After its consumption by atomic carbon, OCS is also efficiently formed until 10^5 yr from HCO and HCS (see Fig. 3c):

$$O + HCS \rightarrow H + OCS \quad (33)$$

$$S + HCO \rightarrow H + OCS. \quad (34)$$

For the remainder of the simulation, HCO^+ is formed efficiently from reaction of H_3^+ with CO, and reacts with OCS:

$$OCS + HCO^+ \rightarrow CO + HOCS^+. \quad (35)$$

However, OCS abundance remains stable at this time because of reaction (28).

In the 0DS300LEDC case, C_4H_2 and C_2H_2 thermally desorb from the grain mantle. Both these species react initially with atomic carbon with reaction rates higher of more than two orders of magnitude than those of reactions (24), (25), (26) and (27) preventing SO, SO_2 and OCS from abrupt initial consumptions. Therefore, SO and SO_2 form rapidly from reactions (11), (14) and (30) (see Figs 3a and b). When the abundance of reactive oxygen drops around 10^3 yr, their abundances will undergo only small variations. Indeed, as the main reactions ruling SO chemistry are no longer efficient because of the lack of reactive oxygen in the gas phase, reactions that recycle SO via HSO^+ allow its abundances to reach a quasi-static regime until the end of the simulation. For instance, because of the high temperature, the high abundances of evaporated H_2O and CO render efficient the two following reactions:

$$H_2O + HSO^+ \rightarrow H_3O^+ + SO \quad (36)$$

$$CO + HSO^+ \rightarrow HCO^+ + SO. \quad (37)$$

Table 4. Description of the reactive oxygen composition in the gas phase at the first time-step of the hot core simulations (post-collapse). The values display the percentage relative to the total abundance of oxygen.

LEDC	
100 K	300 K
41 per cent	33 per cent
EDC	
100 K	300 K
0.1 per cent	<0.09 per cent

The SO thus formed is then put back in HSO^+:

$$SO + H_3^+ \rightarrow H_2 + HSO^+. \quad (38)$$

As a result, the SO_2 abundance shows only a small increase during the final part of the simulation, mainly due to reaction (30).

The OCS abundance does not vary much in the 0DS300LEDC case (see Fig. 3c). When atomic oxygen is still abundant in the gas phase, OCS is mainly formed through reaction (33). Afterwards OCS is destroyed by secondary UV photons to form S and CO, and by H_3^+ through

$$OCS + H_3^+ \rightarrow H_2 + HOCS^+. \quad (39)$$

$HOCS^+$ then recombines electronically to form either CS and OCS, which explains why the latter abundance decreases slowly.

SO, SO_2 and OCS in the EDC cases

The bottom panel of Fig. 3 displays the abundances of SO, SO_2 and OCS in both EDC cases. On the one hand, it appears that the chemistry of these species does not depend as much on the temperature as in the LEDC cases. This can be explained by the poor abundance of reactive oxygen, especially atomic oxygen, in the gas phase in the EDC cases compared with the LEDC cases. Table 4 displays the amount of reactive oxygen (relative to that of total oxygen) in the gas phase at the first time-step of each hot core simulation. It shows that in the LEDC cases at least 33 per cent of the total amount of oxygen is under reactive form in the gas phase, against at most 0.1 per cent in the EDC cases.

On the other hand, the chemistry of SO, SO_2 and OCS looks relatively inert, except for the last part of the simulation ($t > 10^5$ yr). Indeed, in the 0DS100EDC case, SO and SO_2 (see Figs 3d and e) are at first slowly formed through reactions (14) and (30), respectively. As the abundance of HCNS grows from the evaporated NS (accumulated on the grain during the dense parent cloud phase; see Table 2) through

$$NS + CH_2 \rightarrow HCNS + H, \quad (40)$$

the abundance of SO grows steeper from 10^4 yr because of reaction (6). Finally, after 10^6 yr, SO is consumed by CH through reactions (28) and (29). The strong link of SO_2 with SO via reaction (30), coupled with reaction (31), makes its abundance drop at the same time. Regarding OCS (see Fig. 3f), its abundance grows at first in the 0DS100EDC case from reaction (22), then from reaction (34) after 10^4 yr. Towards the end of the simulation, as for SO and SO_2, OCS is destroyed by CH via

$$OCS + CH \rightarrow H + CO + CS. \quad (41)$$

In the 0DS300EDC case, the chemistry of SO, SO_2 and OCS differs from the 0DS100EDC case in two main ways. First, the abundance of OH decreases much faster in the 0DS300EDC case (see Fig. 2f), diminishing even more the quantity of reactive oxygen in the gas phase, causing the abundances of SO, SO_2 and OCS to remain relatively constant during at least the first 10^5 yr of the simulation. Secondly, CH is much less abundant at 300 K (by two to three orders of magnitude) because it is effectively destroyed by evaporated H_2O and C_2H_2:

$$CH + H_2O \rightarrow H + H_2CO \quad (42)$$

$$CH + C_2H_2 \rightarrow H + c - C_3H_2. \quad (43)$$

Hence, SO and SO_2 abundances continue to increase at the end of the simulation (see Figs 3d and e) and do not decrease as in the 0DS100EDC case. However, the lack of CH does not prevent the late-time decrease of OCS (see Fig. 3f), which is ruled by the same reactions as in the 0DS300LEDC case, namely its photodissociation by secondary UV photon and reaction (39).

H_2S, H_2CS and CS in the LEDC cases

Fig. 4 is the same as Fig. 3 but for H_2S, H_2CS and CS. In the 0DS100LEDC case, as for SO, SO_2 and OCS, H_2S and H_2CS (see Figs 4a and b) are both initially destroyed by atomic carbon via the following reactions:

$$H_2S + C \rightarrow H + HCS \quad (44)$$

$$H_2CS + C \rightarrow H + HC_2S \quad (45)$$

$$\rightarrow CS + CH_2. \quad (46)$$

The following increase in H_2S abundance is mainly due to two coupled reactions:

$$CH_2SH + N \rightarrow H_2S + HCN \quad (47)$$

$$HCN + H_3S^+ \rightarrow H_2S + HCNH^+. \quad (48)$$

Indeed, CH_2SH evaporates slowly from the grain surface in the physical conditions of the simulation. Reacting with atomic nitrogen via reaction (47), it forms both H_2S and HCN. The latter then also forms H_2S. The combination of these two reactions explains the steep increase in H_2S abundance between 10 and 10^5 yr. Afterwards, it decreases from the following ion-neutral reactions:

$$H_2S + HCO^+ \rightarrow CO + H_3S^+ \quad (49)$$

$$H_2S + SO^+ \rightarrow H_2O + S_2^+. \quad (50)$$

Towards the end of the simulation, H_2S is efficiently produced by the electronic recombination of $H_3S_2^+$, provided by the following reaction mechanism:

$$S + HS \rightarrow S_2 \xrightarrow{HCO^+} HS_2^+ \xrightarrow{H_2} H_3S_2^+. \quad (51)$$

This mechanism is made efficient by the increase of the abundance of HS during this period of time.

H_2CS gas-phase chemistry at 100 K (in both LEDC and EDC cases; see Figs 4b and e, respectively) is intertwined with its grain

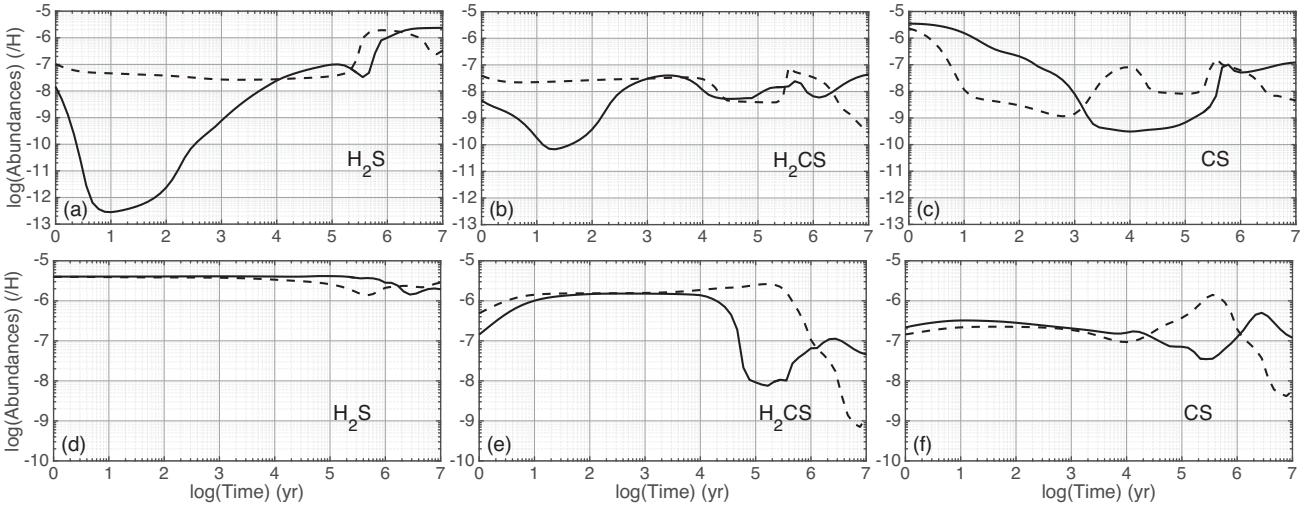

Figure 4. Abundances of H_2S, H_2CS and CS relative to H as a function of time for hot core conditions: $n_H = 2 \times 10^7$ cm^{-3} and $T = 100$ K (solid line) and 300 K (dashed line), and for LEDC (top panel) and EDC (bottom panel) pre-collapse compositions.

chemistry because the temperature is not high enough for its complete thermal desorption from grain ices. Hence, after its destruction by atomic carbon, H_2CS grows from

$$S + CH_3 \rightarrow H_2CS + H. \quad (52)$$

Then its abundance decreases from destruction by $HCNH^+$ in the gas phase, as well as by hydrogenation in the grain bulk. Indeed, the latter contributes to the depletion of H_2CS from the gas phase at this time because the chemistry has reached adsorption/desorption equilibrium. The reactions in question are, respectively,

$$H_2CS + HCNH^+ \rightarrow H_3CS^+ + HCN \quad (53)$$

$$b - H_2CS + b - H \rightarrow b - CH_2SH, \quad (54)$$

where the prefix 'b-' denotes the bulk species. Afterwards, H_2CS abundance increases again, mainly from the electronic recombination of H_3CS^+ and reaction (52).

Contrary to the other S-bearing species studied in this paper, CS is not destroyed by atomic carbon during the early phase of the simulation (see Fig. 4c). It is instead destroyed during a longer period of time (approximately 10^4 yr) by atomic oxygen, contributing efficiently to lock gas-phase oxygen into CO via

$$CS + O \rightarrow S + CO. \quad (55)$$

CS abundance then grows mainly from reaction (25) as well as from the following reaction mechanism:

$$S + CH_2 \rightarrow HCS \xrightarrow{S} CS_2 \xrightarrow{H} CS. \quad (56)$$

As previously observed, atomic carbon is preferentially consumed by evaporated hydrocarbon in the 0DS300LEDC case and therefore has a limited impact on sulphur chemistry compared to the 0DS100LEDC case. Hence, H_2S (see Fig. 4a) is first destroyed by atomic hydrogen and oxygen for 10^3 yr via

$$H_2S + H \rightarrow H_2 + HS \quad (57)$$

$$H_2S + O \rightarrow H_2 + OH. \quad (58)$$

H_2S is after formed by the electronic recombination of $H_3S_2^+$ provided by a similar reaction mechanism as (51), except that instead of HCO^+, it is the H_3O^+ ion that mainly reacts with S_2 to form HS_2^+. Indeed, H_3O^+ is much more abundant in the gas phase at 300 K than at 100 K because it comes mainly from H_2O, which is totally evaporated from grain at this temperature. Furthermore, it is H_3O^+ that destroys H_2S at the end of the simulation:

$$H_2S + H_3O^+ \rightarrow H_2O + H_3S^+. \quad (59)$$

At 300 K, H_2CS is fully depleted from the grain surface and bulk and is affected only by gas-phase chemistry (see Fig. 4b). Partially consumed by atomic carbon during the first 10 yr, it is then formed mainly through reaction (52) and destroyed by reaction (53).

In the 0DS300LEDC case, CS is also initially destroyed by atomic oxygen via reaction (55) (see Fig. 4c), but for a shorter time than in the 0DS100LEDC case. The increase in its abundance at 10^3 yr is mostly due to a reaction mechanism starting from the evaporated C_4H_2:

$$C_4H_2 + S^+ \rightarrow HC_4S^+ \xrightarrow{e^-} C_3S \xrightarrow{O} CCS \xrightarrow{S,N} CS. \quad (60)$$

Then CS is mainly destroyed by $HCNH^+$ via

$$CS + HCNH^+ \rightarrow HCN + HCS^+. \quad (61)$$

Finally, the last increase in its abundance is due to the reaction mechanism (56).

H_2S, H_2CS and CS in the EDC cases

In the EDC cases and prior to collapse, H_2S in icy grain bulk is the second reservoir of sulphur, containing 26 per cent of the total amount of sulphur (see Table 2). Hence, its abundance in both EDC cases is generally higher than in the LEDC cases. Moreover, in the 0DS100EDC case (see Fig. 4d), H_2S initially forms efficiently from its abundant reservoirs counterpart HS via

$$HS + HS \rightarrow S + H_2S. \quad (62)$$

It is also produced during most of the simulation from the slow evaporation of methanol, which is the fourth reservoir of oxygen

in the EDC case (see Table 2), and through the following reaction mechanism:

$$CH_3OH + CN \rightarrow CH_2OH \xrightarrow{S} H_2CO \xrightarrow{H_3S^+} H_2S. \quad (63)$$

Towards the end, H_2S is destroyed via reaction (49).

In the 0DS100EDC case (see Fig. 4e), H_2CS is first formed via reaction (52) as well as from methanol slow depletion with the following reaction mechanism, similar to reaction (63):

$$CH_3OH + CN \rightarrow CH_2OH \xrightarrow{S} H_2CS. \quad (64)$$

As in the 0DS100LEDC case, H_2CS chemistry is afterwards linked with its grain chemistry via reactions (53) and (54), making its abundance drop at 10^5 yr. At the end of the simulation, H_2CS abundance increases again from reaction (52) and electronic recombination of H_3CS^+.

Because of the small amount of reactive oxygen in the EDC cases compared to the LEDC cases (see Table 4), CS is not destroyed by atomic oxygen at the beginning of the simulation (see Fig. 4e). At 100 K, it is instead formed rapidly via

$$HCS + H \rightarrow CS + H_2, \quad (65)$$

with HCS coming from the small fraction of H_2S destroyed by reaction (44). Afterwards, CS is destroyed for a few 10^5 yr by OH and HS via reaction 22 and

$$CS + HS \rightarrow CS_2 + H. \quad (66)$$

When CS_2 abundance is high enough, it is hydrogenated back into CS, causing the abundance of the latter to grow again at the end of the simulation.

In the 0DS300EDC case, all the methanol is directly depleted in the gas phase and rapidly forms CH_3 through many different reactions. Hence, as CH_3 abundance is rapidly much higher than in the 0DS100EDC case, H_2S is mainly destroyed at 300 K via (see Fig. 4d)

$$H_2S + CH_3 \rightarrow HS + CH_4. \quad (67)$$

This high abundance of CH_3 in the gas phase also causes H_2CS to be efficiently formed for a few 10^5 yr by reaction (52) (see Fig. 4e). Afterwards, as in the 0DS300LEDC case, the steep decrease of its abundance is mainly due to reaction (53).

Finally, CS chemistry in the 0DS300EDC case is similar to the 0DS100EDC case, except for the fact that OH abundance at 300 K is much lower than at 100 K (see Fig. 4f). Hence, CS is mainly destroyed by reaction (66). Moreover, as CS_2 abundance grows faster at 300 K than at 100 K, the peak in CS abundance happens sooner in the 0DS300LEDC case. At the end, CS is destroyed like H_2CS, by $HCNH^+$ via reaction (61).

3.1.3 Comparisons to observations

The species studied in this section have been detected in many hot cores and corinos, and their respective observed abundances present differences among sources that can go as high as three orders of magnitude (see for example, table 5 of Wakelam et al. 2004a, and references therein). These variations are often explained by differences among the ages of the sources, or among the temperatures of their respective hot cores or corinos (see discussion in Herpin et al. 2009). Therefore, it would be complex, as well as out of the scope of the present study, to quantitatively compare our results to observations. Qualitatively, however, we can raise the two following points.

(i) The total amount of sulphur observed in massive hot cores generally accounts only for a small part of its cosmic abundance (around 0.1 per cent; see Hatchell et al. 1998; van der Tak 2004; Wakelam et al. 2004a; Herpin et al. 2009), which contrasts with our modelling results where most of the sulphur appears to be in the form of SO, SO_2, H_2S and OCS at the ages that are expected for such objects. Uncertainties on massive hot core observations due to the fact that they are mostly very distant sources, and therefore not spatially resolved, as well as uncertainties on our high-temperature network could explain these discrepancies. However, among this type of source, the hot core of Orion KL presents a high abundance of H_2S of 2.5×10^{-6}, accounting for more than 15 per cent of the total amount of sulphur (Minh et al. 1990), as well as higher abundances of SO and SO_2 than in other massive hot cores (Sutton et al. 1995). It appears that, even if our models fail to reproduce the observed abundances of these molecules for most massive hot core observations, both our EDC models can reproduce the Orion KL abundances of H_2S, SO and SO_2 within one order of magnitude in a range of time acceptable for this structure, between 10^4 and 10^6 yr. However, in this range of time, the models tend to overestimate the abundances of OCS, CS and H_2CS, which suggests that work still has to be done regarding the modelling of the chemistry of these species.

(ii) The only hot corinos towards which all the S-bearing species studied in this paper have been observed is IRAS 16293–2422. The observed abundances of SO, SO_2, OCS, H_2CS and H_2S in the dense inner part of its envelope ($\leq$150 au; see table 7 of Schöier et al. 2002) can be reproduced within one order of magnitude by both our LEDC models in a range of time compatible with that derived by Schöier et al. (2002), between a few 10^3 and a few 10^4 yr. This result would suggest that IRAS 16293–2422 has formed in a parent cloud that would have collapsed at an age of approximately 10^5 yr.

These results suggest that, following our previous paper (Vidal et al. 2017), our model can reproduce observations of S-bearing molecules in H_2S-rich hot cores and in hot corinos using – as an initial abundance of sulphur – its cosmic abundance. However, work still has to be conducted regarding our high-temperature network, especially for OCS, H_2CS and CS.

3.2 One-dimensional static models

In this section, we study the results of the two one-dimensional static simulations whose parameters are described in Section 2.4 and Table 3. The goal is to evaluate the impact of the pre-collapse chemical composition of the parent cloud on the computed abundances of the main S-bearing species SO, SO_2, OCS, H_2S, H_2CS and CS. Both LEDC and EDC simulations were run for a period of 3.5×10^5 yr so as to make the results comparable to those of the zero-dimensional dynamic simulations presented in Section 3.3.

Fig. 5 displays the abundances of each of these species for both 1DSLEDC (solid lines) and 1DSEDC (dashed lines) pre-collapse compositions. For a radius greater than 300 au, which corresponds to the outermost and coldest ($T < 50$ K) part of the envelope of the protostar, most considered species present only small local differences in their abundances between the LEDC and EDC cases. Only SO_2 presents significant differences that can go to more than three orders of magnitude while other species display differences smaller than one order of magnitude (see Fig. 5b).

In the inner part of the envelope ($R < 300$ au) where the temperature goes from 50 to 200 K (see the right panel of Fig. 1), all

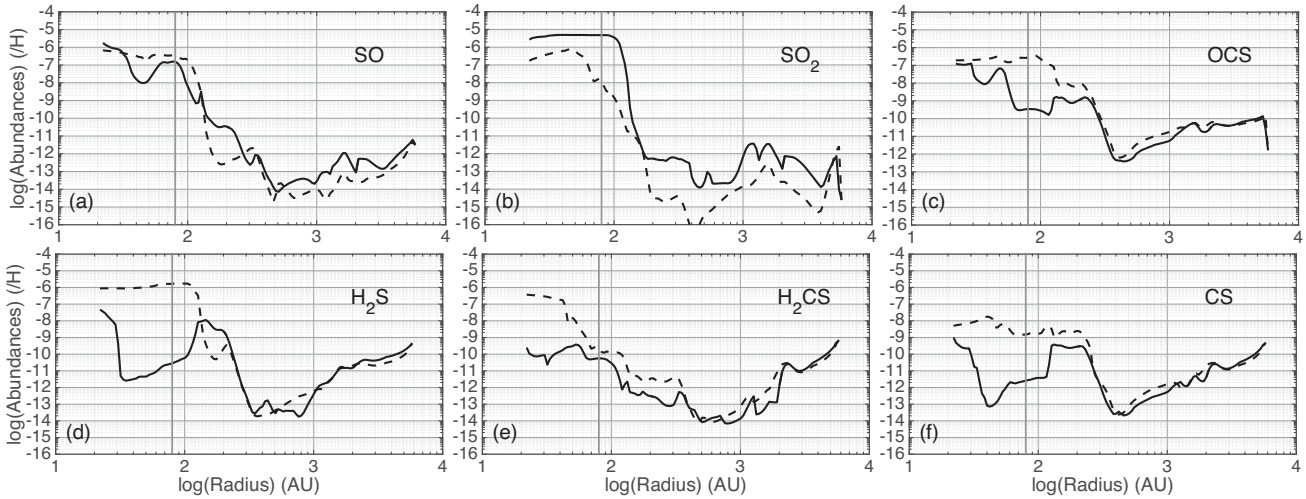

Figure 5. Abundances of SO, SO_2 and OCS (top panel) and H_2S, H_2CS and CS (bottom panel), relative to H as a function of the radius to the star IRAS 16293–2422 according to the one-dimensional structure of Crimier et al. (2010), for the LEDC (solid line) and EDC (dashed line) pre-collapse compositions. Both models were run for a period of 3.5×10^5 yr so the results would be comparable to those of the zero-dimensional dynamic simulations. The vertical grey line represent the hot core spatial limit $R_{HC} = 80$ au, $T > 100$ K.

species abundances show significant differences between the LEDC and EDC pre-collapse compositions. These differences can go from two to more than six orders of magnitude. Within the hot core limits (delimited by a vertical grey line in Fig. 5 at $R_{HC} < 80$ au, $T > 100$ K), the species that are most sensitive to the pre-collapse composition appear to be H_2S, H_2CS, and CS with differences of more than three orders of magnitude (see Figs 5d, e and f, respectively). For H_2S, these differences are explained by its dependence on the parent cloud evolution time. Indeed, in the EDC case, H_2S in icy grain bulk is the second reservoir of sulphur in the pre-collapse composition, containing 26 per cent of the total amount of sulphur, whereas in the LEDC case, it only contains 5 per cent (see Table 2). Hence, in the inner part of the envelope and the hot core, where the temperature is high enough for H_2S thermal desorption, its abundance is much higher than in the LEDC case. Moreover, Fig. 4 shows that, in that case, H_2S is not efficiently destroyed in the gas phase. Regarding H_2CS, this species efficiently forms at high temperature in the gas phase from CH_3, via reaction (52), which is much more abundant in the EDC case because of evaporated methanol and hydrocarbons accumulated on the grains during the parent cloud evolution. Finally, in the EDC case, CS is not as efficiently destroyed in the gas phase as in the LEDC case (see Fig. 4) because of the low abundance of reactive oxygen (see Table 4).

We can finally highlight that our one-dimensional static models show that the pre-collapse composition of the parent cloud appears to be critical for the sulphur-bearing species in hot core physical conditions. Indeed, we can see from Fig. 5 that a hot core that formed from a young parent cloud will be poor in H_2S and rich in SO_2, while a hot core formed from a more evolved parent cloud would be rich in H_2S and H_2CS.

3.3 Zero-dimensional dynamic model

In this section, we carry out the same study as in the previous section but for the zero-dimensional dynamic simulations 0DDLEDC and 0DDEDC described in Section 2.5 and Table 3.

Fig. 6 is the same as Fig. 5 but for the zero-dimensional dynamic simulations. In this figure, it is particularly striking that the pre-collapse chemical composition of the parent cloud appears to have little or no effect on the abundances of the considered S-bearing species. Only SO presents a significant difference in the hot core (delimited by a vertical grey line in Fig. 6 at $R_{HC} < 135$ au, $T > 100$ K), and even this difference is no more than a factor of 7 (see Fig. 6a). A possible explanation for this lack of differences would be that the free-fall time considered in these simulations is long enough for both models to evolve towards the same chemical composition. Indeed, if the initial pre-collapse chemical composition has enough time to evolve in an environment cold enough for species not to evaporate, it will tend towards a state similar to the EDC case (i.e. with an evolved grain surface and bulk chemistry), notably with most of the sulphur transformed into H_2S and OCS on the grains. Hence, the hot core chemical composition of both 0DDLEDC and 0DDEDC would be very similar.

Moreover, the modification we made to the density profile of the model would tend to accelerate the chemistry and adsorption of species on the grains and therefore reduce the chemical time-scale. We expect that by using the original model of Aikawa et al. (2008) we would obtain more differences and thus a more important impact of the pre-collapse chemical composition on the hot core chemistry.

4 DISCUSSION

4.1 Modification of the density profile of the dynamic model

In order to evaluate the impact of the modification of the density radial profile for our zero-dimensional dynamic model on sulphur chemistry, we run the 0DDLEDC and 0DDEDC cases, but this time using the original physical structure of Aikawa et al. (2008). Fig. 7 is therefore the same as Fig. 6, but for the models run with the original density structure of Aikawa et al. (2008). As expected, the results displays larger differences between the LEDC and EDC pre-collapse compositions cases, which can be explained by a slower chemistry due to lower density. Moreover, as discussed in Wakelam et al. (2014), lower densities tend to decrease adsorption of species on grains (and consequently depletion), and therefore enhance gas-phase chemistry at low temperature, which explains why the abundances of the studied species are higher in the envelope in the original structure case. However, the resulting abundances

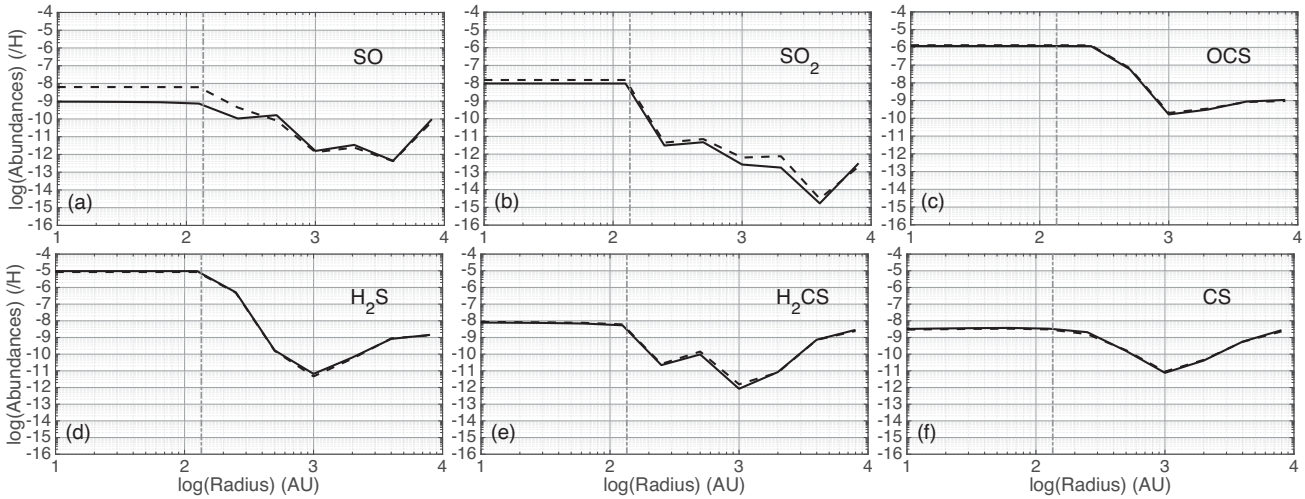

Figure 6. Abundances of SO, SO_2 and OCS (top panel) and H_2S, H_2CS and CS (bottom panel), relative to H as a function of the radius to the star IRAS 16293–2422 according to the modified structure of Aikawa et al. (2008), for the LEDC (solid line) and EDC (dashed line) pre-collapse compositions. The vertical grey dashed line represents the hot core spatial limit $R_{HC} = 135$ au, $T > 100$ K.

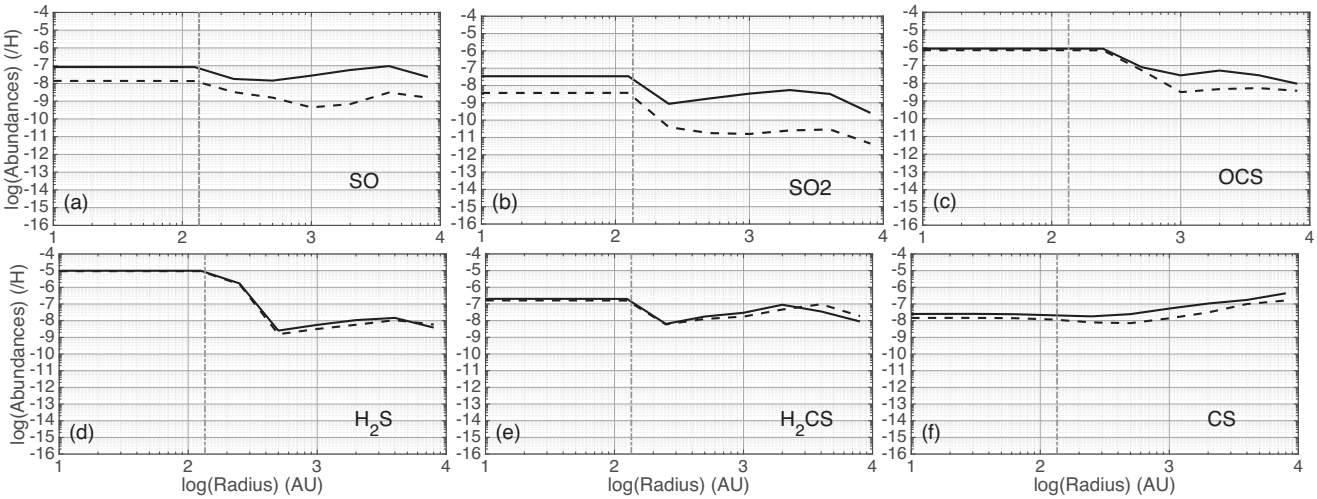

Figure 7. Abundances of SO, SO_2 and OCS (top panel) and H_2S, H_2CS and CS (bottom panel), relative to H as a function of the radius to the star IRAS 16293–2422 according to the original structure of Aikawa et al. (2008), for the LEDC (solid line) and EDC (dashed line) pre-collapse compositions. The vertical grey dashed line represents the hot core spatial limit $R_{HC} = 135$ au, $T > 100$ K.

in the hot core do not change drastically (at most slightly more than one order of magnitude) and are even the same for OCS and H_2S (see Figs 7c and d, respectively). As discussed in Section 3.3, this could be explained by a long free-fall time, which would give the chemistry enough time for H_2S and OCS to accumulate on the grains before thermal depletion in the hot core. More complete studies of the effect of density and free-fall time on the chemistry of a collapsing envelopes and hot cores will be conducted in the future.

4.2 H_2S and the initial abundance of sulphur

This study was conducted in light of the previous results we obtained regarding the sulphur reservoir in dark clouds (Vidal et al. 2017), namely that depending on the age of the cloud, the reservoir of sulphur could be either atomic sulphur in the gas phase (LEDC case) or H_2S and HS in icy grain bulk nearly equally sharing more than 55 per cent of the total amount of sulphur (EDC case). Another result was that the NAUTILUS model could reproduce the S-bearing observations in the dark cloud TMC-1 using as an initial abundance of sulphur its cosmic abundance, or three times depleted. Hence, throughout this paper, we present results obtained using the cosmic abundance of sulphur of 1.5×10^{-5} (Jenkins 2009). With this initial abundance of sulphur, the H_2S abundances obtained in the hot core in the dynamic simulation with the modified as well as the original structure from Aikawa et al. (2008) is as high as 10^{-5}. Such a high abundance of H_2S is not consistent with the abundance derived from the observation of IRAS 16293–2422 (2.7×10^{-7}; see Wakelam et al. 2004a). On the one hand, to understand why the model overestimates the H_2S abundance, we ran all the models presented in this paper with an initial abundance of 5×10^{-6}. It should be noted that it only changes the presented results quantitatively, linearly diminishing the abundances of the studied species by approximately a factor of 3. Regarding H_2S in the dynamical case, this initial depletion of sulphur allows an estimation of its abundance in the hot

Table 5. Comparison of the abundances obtained in the LEDC case. where $a(b)$ stands for $a \times 10^b$.

Species	$(n_i/n_H)_{1DSLEDC}$	$(n_i/n_H)_{0DDLEDC}$
	$R = 50$ au (hot core)	
SO	5.7(−8)	9.0(−10)
SO_2	1.4(−5)	9.5(−9)
OCS	3.0(−7)	1.2(−6)
H_2S	1.2(−11)	9.5(−6)
H_2CS	7.4(−10)	7.6(−9)
CS	1.2(−12)	3.3(−9)
	$R = 500$ au (envelope)	
SO	2.3(−14)	1.6(−10)
SO_2	1.2(−13)	4.7(−12)
OCS	2.2(−12)	5.8(−8)
H_2S	1.1(−13)	1.7(−10)
H_2CS	2.7(−14)	1.4(−10)
CS	1.2(−13)	1.7(−10)

core to be slightly overestimated around 3×10^{-6}, but it could be considered in accordance with the observations (within a margin of one order of magnitude).

On the other hand, the overestimation of H_2S that we find could be a result of the efficient formation path due to slowly evaporating CH_2SH and CH_3OH at 100 K studied in Section 3.1. This contradicts previous theoretical and laboratory studies that predict that in the high-temperature gas phase, the H_2S evaporated from grain ices is preferentially destroyed to form SO and SO_2, or molecules with two S atoms, such as H_2S_2 or HS_2 (Charnley 1997; Wakelam et al. 2004b; Druard & Wakelam 2012; Esplugues et al. 2014; Martín-Doménech et al. 2016). Hence, this result could suggest missing efficient destruction gas-phase reactions in the H_2S chemistry in our network.

4.3 Sensitivity to the type of simulation

One goal of this paper is to highlight the differences that can appear when using two types of simulations to model the same hot core. In order to do so, we have used a one-dimensional static model and a zero-dimensional dynamic model of IRAS 16293–2422. Our results show that our one-dimensional model favours a hot core sulphur chemistry dominated by SO_2 and SO in the LEDC case and by H_2S in the EDC case, while our zero-dimensional dynamic model displays in both cases high abundances of H_2S and OCS and low abundances of SO_2 and SO. Table 5 displays the abundances obtained for both types of models in the LEDC case, at 50 au (in the hot core) and at 500 au (in the envelope). In light of the difference in abundance that exists for a given species between the two type of models, we can easily make a conclusion about the sensitivity to the type of simulation used to compute the chemistry of a hot core and its collapsing envelope. Especially in the hot core, these differences can reach as much as six orders of magnitude, rendering critical the choice of model used to compare results with possible observations or related works.

4.4 Importance of the pre-collapse chemical composition

The observations of S-bearing species in hot cores are still a puzzling issue, as a large variety of sulphur compositions have been observed towards different hot cores and therefore no global trend has yet been found (see fig. 5 of Woods et al. 2015, and references therein). However, a given set of hot cores can present similar sulphur compositions (see for example, Minh 2016), which would suggest similar evolutionary stages. In this paper we have investigated the importance of the pre-collapse chemical composition on the hot core chemistry of S-bearing species. Our results on zero-dimensional and one-dimensional simulations (Sections 3.1 and 3.2) support the fact that, given the fast evolution of sulphur chemistry in the parent cold clouds, the pre-collapse chemical composition is a critical parameter for hot core simulations. This could partially explain the absence of a global trend for sulphur compositions in observed hot cores from different parent clouds, as well as supporting the fact that for parent clouds that collapse at similar ages and physical environments, hot cores can have similar sulphur compositions. However, the study of our dynamical simulation (Section 3.3) raises the question of the role of the free-fall time on sulphur evolution, which would also explain the similar composition of different hot cores, especially those where H_2S and OCS are found to be more abundant than the other species (see for example, Herpin et al. 2009).

5 CONCLUSIONS

In this paper, we aimed to take a comprehensive look at the chemistry of sulphur in hot cores. In order to do so, we have conducted an extensive study with simple zero-dimensional models of the chemistry of the main S-bearing species observed towards hot cores, namely SO, SO_2, OCS, H_2S, H_2CS and CS. We have presented and compared the results from two types of simulations (one-dimensional static and zero-dimensional dynamic), in order to highlight the sensitivity of chemistry to the choice of model used in astrochemical studies.

Our zero-dimensional extensive study revealed four main results:

(i) The total amount of reactive oxygen in the gas phase depends critically on the pre-collapse composition of the hot core (see Table 4) as well as the temperature.

(ii) Sulphur chemistry in hot and dense gas also depends greatly on the pre-collapse composition, mainly because of its impact on reactive atomic oxygen, carbon and hydrogen, which all participate actively in most of the sulphur chemistry in such environments.

(iii) Sulphur chemistry in hot and dense gas depends greatly on the temperature, partly because it is directly and indirectly linked with hydrocarbon evaporated from grain ices, and their main destruction products CH_2 and CH_3.

(iv) We found efficient paths of formation of gas-phase H_2S that could be responsible for its overestimation in most of our hot core results. Studies of the gas-phase chemistry of this species need to be continued to ensure the relevance of our network.

Our study of the one-dimensional static and zero-dimensional dynamic models led to the following conclusions:

(i) The pre-collapse chemical composition of the parent cloud is a key parameter for one-dimensional static simulations of sulphur chemistry in hot cores. Indeed, the computed abundances showed that it can imply differences up to six orders of magnitude for a given species in the hot core. However, the pre-collapse composition appears to have only a small impact on the chemical composition of the envelope. Finally, our one-dimensional model shows that a hot core that was formed from a young parent cloud will be poor in H_2S and rich in SO_2, while a hot core formed from a more evolved parent cloud would be rich in H_2S and H_2CS.

(ii) The zero-dimensional dynamic simulations conducted in this paper have revealed only small differences between the results of the less evolved and the evolved pre-collapse chemical composition, showing only a weak dependence of the hot core sulphur chemistry on the pre-collapse composition. Indeed, for both cases, the model predicts high abundances of H_2S and OCS and low abundances of SO_2 and SO. However, this result is thought to be due to the long free-fall time used in our model, which would allow enough time for sulphur to be adsorbed on to grains and to form mainly H_2S and OCS in the envelope before thermal depletion. We expect that for a shorter free-fall time the differences between the two pre-collapse composition cases would be larger. Future work will focus on this importance of the free-fall time, as along with the pre-collapse chemical composition, it could explain the large variety of abundances of S-bearing species observed in hot cores.

The comparison between the one-dimensional static and zero-dimensional dynamic models has displayed large differences between the computed abundances, which can be as high as six orders of magnitude in the hot core. This result highlights the sensitivity to the choice of simulations in astrochemical studies, especially when comparing results with observations, or with results from other papers.

ACKNOWLEDGEMENTS

This work has been funded by the European Research Council (Starting Grant 3DICE, grant agreement 336474). The authors are also grateful to the CNRS programme, Physique et Chimie du Milieu Interstellaire (PCMI), for partial funding of their work.

REFERENCES

Aikawa Y., Wakelam V., Garrod R. T., Herbst E., 2008, ApJ, 674, 984
Cazaux S., Caselli P., Tielens A. G. G. M., LeBourlot J., Walmsley M., 2005, J. Phys. Conf. Ser., 6, 155
Ceccarelli C., Hollenbach D. J., Tielens A. G. G. M., 1996, ApJ, 471, 400
Chaabouni H., Bergeron H., Baouche S., Dulieu F., Matar E., Congiu E., Gavilan L., Lemaire J. L., 2012, A&A, 538, A128
Chang Q., Cuppen H. M., Herbst E., 2007, A&A, 469, 973
Charnley S. B., 1997, ApJ, 481, 396
Crimier N., Ceccarelli C., Maret S., Bottinelli S., Caux E., Kahane C., Lis D. C., Olofsson J., 2010, A&A, 519, A65
Druard C., Wakelam V., 2012, MNRAS, 426, 354
Esplugues G. B., Viti S., Goicoechea J. R., Cernicharo J., 2014, A&A, 567, A95
Garrod R. T., Herbst E., 2006, A&A, 457, 927
Garrod R. T., Pauly T., 2011, ApJ, 735, 15
Garrod R. T., Wakelam V., Herbst E., 2007, A&A, 467, 1103
Graedel T. E., Langer W. D., Frerking M. A., 1982, ApJS, 48, 321
Harada N., Herbst E., Wakelam V., 2010, ApJ, 721, 1570
Hatchell J., Thompson M. A., Millar T. J., MacDonald G. H., 1998, A&A, 338, 713
Herbst E., van Dishoeck E. F., 2009, ARA&A, 47, 427
Herpin F., Marseille M., Wakelam V., Bontemps S., Lis D. C., 2009, A&A, 504, 853
Hickson K. M., Wakelam V., Loison J.-C., 2016, Molecular Astrophysics, 3, 1
Hincelin U., Wakelam V., Hersant F., Guilloteau S., Loison J. C., Honvault P., Troe J., 2011, A&A, 530, A61
Hincelin U., Commerçon B., Wakelam V., Hersant F., Guilloteau S., Herbst E., 2016, ApJ, 822, 12
Holdship J. et al., 2016, MNRAS, 463, 802
Ivezic Z., Elitzur M., 1997, MNRAS, 287, 799
Jenkins E. B., 2009, ApJ, 700, 1299
Karssemeijer L. J., Cuppen H. M., 2014, A&A, 569, A107
Kurtz S., Cesaroni R., Churchwell E., Hofner P., Walmsley C. M., 2000, in Mannings V., Boss A. P., Russell S. S., eds, Protostars and Planets IV. Univ. Arizona Press, Tuscon, AZ, p. 299
Loison J.-C. et al., 2016, MNRAS, 456, 4101
Loison J.-C. et al., 2017, MNRAS, 470, 4075
Majumdar L., Gratier P., Vidal T., Wakelam V., Loison J.-C., Hickson K. M., Caux E., 2016, MNRAS, 458, 1859
Martín-Doménech R., Jiménez-Serra I., Muñoz Caro G. M., Müller H. S. P., Occhiogrosso A., Testi L., Woods P. M., Viti S., 2016, A&A, 585, A112
Masunaga H., Inutsuka S.-i., 2000, ApJ, 531, 350
Minh Y. C., 2016, J. Phys. Conf. Ser., 728, 052007
Minh Y. C., Irvine W. M., McGonagle D., Ziurys L. M., 1990, ApJ, 360, 136
Neufeld D. A., Wolfire M. G., Schilke P., 2005, ApJ, 628, 260
Oya Y., Sakai N., López-Sepulcre A., Watanabe Y., Ceccarelli C., Lefloch B., Favre C., Yamamoto S., 2016, ApJ, 824, 88
Podio L. et al., 2015, A&A, 581, A85
Prasad S. S., Tarafdar S. P., 1983, ApJ, 267, 603
Ruaud M., Wakelam V., Hersant F., 2016, MNRAS, 459, 3756
Sakai N. et al., 2014, Nature, 507, 78
Schöier F. L., Jørgensen J. K., van Dishoeck E. F., Blake G. A., 2002, A&A, 390, 1001
Sutton E. C., Peng R., Danchi W. C., Jaminet P. A., Sandell G., Russell A. P. G., 1995, ApJS, 97, 455
Tieftrunk A., Pineau des Forets G., Schilke P., Walmsley C. M., 1994, A&A, 289, 579
van der Tak F. F. S., 2004, in Burton M. G., Jayawardhana R., Bourke T. L., eds, Proc. IAU Symp. Vol. 221, Star Formation at High Angular Resolution. Kluwer, Dordrecht, p. 59
Vidal T. H. G., Loison J.-C., Jaziri A. Y., Ruaud M., Gratier P., Wakelam V., 2017, MNRAS, 469, 435
Viti S., Caselli P., Hartquist T. W., Williams D. A., 2001, A&A, 370, 1017
Wakelam V., Herbst E., 2008, ApJ, 680, 371
Wakelam V., Castets A., Ceccarelli C., Lefloch B., Caux E., Pagani L., 2004a, A&A, 413, 609
Wakelam V., Caselli P., Ceccarelli C., Herbst E., Castets A., 2004b, A&A, 422, 159
Wakelam V., Hersant F., Herpin F., 2011, A&A, 529, A112
Wakelam V., Vastel C., Aikawa Y., Coutens A., Bottinelli S., Caux E., 2014, MNRAS, 445, 2854
Wakelam V. et al., 2015a, ApJS, 217, 20
Wakelam V., Loison J.-C., Hickson K. M., Ruaud M., 2015b, MNRAS, 453, L48
Woods P. M., Occhiogrosso A., Viti S., Kaňuchová Z., Palumbo M. E., Price S. D., 2015, MNRAS, 450, 1256

This paper has been typeset from a TEX/LATEX file prepared by the author.